*Journal of Statistical Physics, Vol. 95, Nos. 1/2, 1999*

# Growth of Ordered Domains in a Computer Model Alloy with Lattice Misfit

**P. Nielaba,[1] P. Fratzl,[2] and J. L. Lebowitz[3]**

*Received May 12, 1998; final October 15, 1998*

We study via Monte Carlo simulations the influence of elastic interactions on the ordering and decomposition of a two-dimensional model binary alloy with antiferromagnetic nearest and ferromagnetic next nearest neighbor type interactions following a quench into the coexistence region. The elastic interaction leads to the development of a platelet morphology for the segregated ordered and disordered regions. A length scale characterizing the coarsening process follows a law of the type $R = a + bt^{1/3}$ with the growth $b$ decreasing with the amount of ordered phase; this appears to be due to the presence of anti-phase boundaries between neighboring domains ordered on different sublattices which are difficult to eliminate. The application of uniaxial external stress results in "rafting" of the domains. Many of the simulation results are in agreement with experimentally observed effects in nickel-base superalloys.

**KEY WORDS:** Model alloy; Monte Carlo; elastic interactions; phase separation; kinetics.

## I. INTRODUCTION

Precipitate micro structures are important for the strength and hardness of many alloys.[1–11] A number of experimental[12–27] and theoretical[6, 28–41] investigations have shown that the development of precipitate morphologies is influenced by elastic interactions (EI) resulting from a lattice misfit between matrix and precipitates and from an externally applied elastic strain.

[1] Institute for Physics, University of Mainz, D-55099 Mainz, Germany, and Institute for Theoretical Physics, University of Saarland, D-66041 Saarbrücken, Germany; permanent address: Theoretical Physics, University of Konstanz, D-78457 Konstanz, Germany.

[2] Erich Schmid Institute of Materials Science, Austrian Academy of Sciences and University of Leoben, Jahnstr. 12, A-8700 Leoben, Austria.

[3] Department of Physics and Mathematics, Rutgers University, Piscataway, New Jersey 08855-0849.



0022-4715/99/0400-0023$16.00/0 

Thus, in Nickel base superalloys[22–26] cuboidal precipitates develop as a result of EI.[21] These cuboids may join into large plates either spontaneously in the coarsening process or, more impressively, as a result of an externally applied uniaxial stress. These processes are reasonably well described by models where anisotropic elastic strains are incorporated into the kinetics of a phase separating system.[6, 29, 31, 39–43] Such models include continuum approaches as well as atomistic computer simulations. In particular, an Ising type model has been developed[35–38] which predicts the growth of plate-like domains oriented perpendicular to the elastically soft directions, in agreement with experiment. The model fails however to reproduce some of the micro-structural details,[21] like narrow channels of disordered phase effectively cutting the plates into a succession of cuboids.

It has been suggested[31] that these channels correspond to wetted anti-phase boundaries (APB's) between variants of atomically ordered precipitates. Such a proposal is very difficult to check experimentally since variants of an ordered phase can only be distinguished in electron microscopy by measuring large specimen areas using atomic resolution, which is generally not possible. Similarly, the Ising model mentioned above did not include the possibility of different atomically ordered domains and cannot, therefore give an answer to this question. On the other hand, it is well known that the precipitation of ordered domains inside a random matrix is strongly influenced by the ordering tendency.[22–26] Simulations of Ising models (not including EI) in which the ordered domains were of two types gave a precipitate morphology strongly dependent on the volume fraction of the disordered domain.[11] This can be interpreted as due to the fact that the disordered phase has always a tendency to wet the surface of the ordered domains.[11]

In the present work, we generalize the previous model[11] by including EI resulting from a different size of the two types of atoms. We then study, via computer simulations, the influence of the ordering tendency of the precipitates on the domain structure and the kinetics both without and with external stress (rafting).

## II. THE MODEL

We consider a system consisting of $N_A$ atoms of type $A$ with radii $R_A$ and $N_B$ atoms of type $B$ with radii $R_B$. The positions of the atoms are labeled by sites on a planar square lattice $\mathscr{L}$ with lattice spacing $a$. There are $N = L^2$ sites ($N = N_A + N_B$) and we use periodic boundary conditions. A spin variable $\gamma(\mathbf{p})$ is assigned at each site $p \in \mathscr{L}$, with $\gamma(\mathbf{p}) = 1$ if there is an $A$-atom at site $\mathbf{p}$ and $\gamma(\mathbf{p}) = -1$ if there is a $B$-atom there. The atoms, which can move off the lattice sites, are connected by elastic springs with

longitudinal ($L_+$) and transverse ($T_+$) stiffness between nearest neighbors and springs with longitudinal stiffness ($L_\times$) between next nearest neighbors. The different sizes of the atoms cause a lattice distortion, as discussed in refs. 35–38. There is also a short range "chemical interaction," $H_{\text{chem}}$, between the atoms corresponding to anti-ferromagnetic (AFM) nearest and ferromagnetic (FM) next nearest neighbor potentials.[11] This has the form of an Ising Hamiltonian:

$$H_{\text{chem}} = J \sum_{\mathbf{p} \in \mathscr{L}} \sum_{j=1,2} \gamma(\mathbf{p})\, \gamma(\mathbf{p} + a\mathbf{e}_j) - \frac{J}{2} \sum_{\mathbf{p} \in \mathscr{L}} \sum_{j=-1,1} \gamma(\mathbf{p})\, \gamma(\mathbf{p} + a(\mathbf{e}_1 + j\mathbf{e}_2)), \qquad J > 0 \tag{1}$$

where $\mathbf{e}_1$ and $\mathbf{e}_2$ are unit vectors in horizontal and vertical direction, respectively.

An energy minimization over the atomic displacements for a given configuration can be performed as in refs. 47, 48, 35–38 and the resulting total Hamiltonian is then given by:

$$H_{\text{tot}} = \frac{1}{2N} \sum_{\mathbf{k} \in BZ} \tilde{\Psi}(\mathbf{k})\, |\tilde{\gamma}(\mathbf{k})|^2 = \frac{1}{2N} \sum_{\mathbf{p},\, \mathbf{p}' \in \mathscr{L}} \Psi(\mathbf{p} - \mathbf{p}')\, \gamma(\mathbf{p})\, \gamma(\mathbf{p}') \tag{2}$$

where $\tilde{\gamma}(\mathbf{k})$ and $\tilde{\Psi}(\mathbf{k})$ are the Fourier transforms of $\gamma(\mathbf{p})$ and the effective pair potential $\Psi(\mathbf{p} - \mathbf{p}')$ respectively,

$$\tilde{\gamma}(\mathbf{k}) = \sum_{\mathbf{p}} \gamma(\mathbf{p})\, e^{i\mathbf{k}\cdot\mathbf{p}}; \qquad \tilde{\Psi}(\mathbf{k}) = \sum_{\mathbf{p}} \Psi(\mathbf{p})\, e^{i\mathbf{k}\cdot\mathbf{p}}$$

and the sum over $\mathbf{k}$ in (2) is taken over the first Brillouin zone of the lattice $\mathscr{L}$.

The effective potential $\Psi(\mathbf{p})$ contains a *long range anisotropic* elastic part $\Psi_{\text{el}}^{\text{eff}}(\mathbf{p})$ which has a form similar to a dipole–dipole interaction and decays like $r^{-2}$ ($r^{-3}$ in 3 dimensions) at large distances $r$. It also contains a short-range part $\Psi_{\text{sh}}(\mathbf{p})$ which has contributions from both the chemical and the elastic interactions. In Fourier space the potential $\tilde{\Psi}(\mathbf{k})$, which is the sum of $\tilde{\Psi}_{\text{sh}}(\mathbf{k}) + \tilde{\Psi}_{\text{el}}^{\text{eff}}(\mathbf{k})$, can be calculated explicitly; see refs. 35–38:

$$\tilde{\Psi}_{\text{sh}}(\mathbf{k}) = 2J \left\{ c_1 + c_2 - c_1 c_2 + \frac{1}{4} \lambda \tilde{\Omega} \right\} \tag{3}$$

$$\tilde{\Psi}_{\text{el}}^{\text{eff}}(\mathbf{k}) = -\frac{1}{2} \lambda J \frac{\tilde{\mathscr{D}}_{22} \tilde{G}_1^2 + \tilde{\mathscr{D}}_{11} \tilde{G}_2^2 - 2\tilde{\mathscr{D}}_{12} \tilde{G}_1 \tilde{G}_2}{\tilde{\mathscr{D}}_{11} \tilde{\mathscr{D}}_{22} - \tilde{\mathscr{D}}_{12}^2} \tag{4}$$

Here $i \in \{1, 2\}$, $c_i = \cos ak_i$, and $s_i = \sin ak_i$, $k_1$ and $k_2$ being the components of the vector $\mathbf{k}$ along the $x$ and $y$ directions of the square lattice, $\lambda = (R_A - R_B)^2/J$,

$$\tilde{\Omega} = \sum_{i=1}^{2} \{(1 - 2\alpha\varepsilon_{ii}^0)(1 + c_i)\, L_+ + [1 - \alpha(\varepsilon_{11}^0 + \varepsilon_{22}^0)](1 + c_1 c_2)\, L_\times\}$$

and

$$\tilde{G}_i = s_i(1 - \alpha\varepsilon_{ii}^0)\, L_+ + [c_{3-i} s_i (1 - \alpha(\varepsilon_{11}^0 + \varepsilon_{22}^0)/2) - c_i s_{3-i} \alpha\varepsilon_{12}^0/2]\, \sqrt{2}\, L_\times$$

$$\tilde{\mathscr{D}}_{ij} = \delta_{ij}\{(1 - c_i)\, L_+ + (1 - c_{3-i})\, T_+ + (1 - c_1 c_2)\, L_\times\} + (1 - \delta_{ij})\, s_1 s_2 L_\times$$

where $\varepsilon_{ij}^0$ is the $(i, j)$-component of the strain tensor and $\alpha \neq 0$ corresponds to non-zero *external* stress, see refs. 37 and 38.

## A. Computer Simulations

For the numerical simulations, we chose[37, 38]

$$\lambda B = 2, \qquad L_+/B = 0.48, \qquad L_\times/B = 0.68, \qquad T_+/B = -0.16$$

where $B$ is the bulk modulus of the material, introduced here in order to make the above parameters dimensionless. A purely external stress $\varepsilon_{11}$ in the $x$-direction corresponds, as shown in refs. 37 and 38, to setting

$$\varepsilon_{12}^0 = 0 \qquad \text{and} \qquad \varepsilon_{22}^0 = -\frac{C_{12}^0}{C_{11}^0}\varepsilon_{11}^0 = -\frac{L_\times - T_+}{L_\times + L_+}\varepsilon_{11}^0 \approx -0.724\varepsilon_{11}^0 \tag{5}$$

For simplicity we also define $\zeta = \alpha\varepsilon_{11}^0$. $\zeta < 0$ corresponds to compressive stress in the $x$-direction, $\zeta > 0$ corresponds to tensile stress in the $x$-direction. In the computer simulations we studied the cases $\zeta = 0$ and $\zeta = 0.1$. An approximate phase diagram of this system with energy (1), i.e., in the absence of EI's, is shown in Fig. 1. The Monte Carlo simulations by Landau[44, 45] for the model without EI show that the phase diagram contains a tricritical point at a tri-critical concentration close to a value at which half of the system is ordered and the other half is disordered. As discussed by Kincaid and Cohen,[46] the corresponding mean field theory provides a phase diagram with a critical end point instead of a tricritical point for the interaction parameters chosen in the present study. The precise location of the phase coexistence boundaries and the critical line is the topic of a

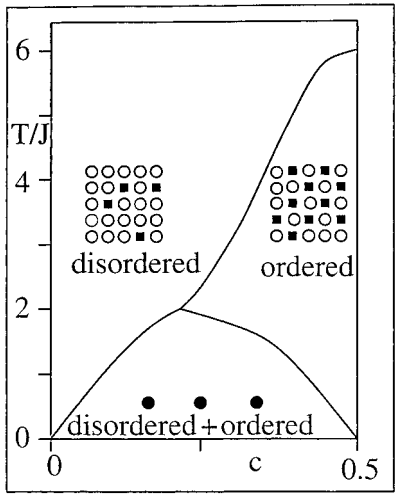


Fig. 1. Schematic equilibrium phase diagram (concentration $c$ of A atoms vs. temperature $T$) for the model A–B alloy, full squares: A-atoms, open circles: B-atoms. The full circles show the conditions at which our MC simulations were performed.

separate study. However, guided by the results of refs. 35 and 36 for the case with FM- and elastic interactions, we expect only relatively small quantitative modifications of the phase diagram of the system without EI, say an increase of the tri-critical temperature of order 10%, due to the added EI's used here.

Computer simulations were performed mainly on a $128 \times 128$ lattice at a temperature, $T = T_c^{is}/4 \approx 0.567 J/k_B$, ($T_c^{is}$ is the critical temperature of the two-dimensional nearest-neighbor AFM Ising model) with ($\zeta = 0.1$) and without ($\zeta = 0$) external stress. Three "alloys" with concentration of (large) A-atoms $c = N_A/N = 0.15$, $c = 0.25$ and $c = 0.35$ were considered. These are all well within the two-phase region between the ordered inter-metallic alloy with stoichiometric composition AB and the disordered B-rich phase; corresponding approximately to volume fractions of the ordered phase $f = 0.3$, 0.5 and 0.7, respectively. The simulations were performed using the algorithm described in refs. 35 and 36. In essence, it amounts to the Metropolis algorithm with Kawasaki dynamics: a nearest neighbor pair is chosen at random and if the exchange of the pair leads to a decrease in total energy, then the exchange is performed, but if it leads to an increase $\delta E$, it is only done with probability $\exp(-\delta E/kT)$. One Monte Carlo step (MCS) consists of one attempted update of every lattice site. Since the interaction potential is long-range, a special updating procedure (described in ref. 35) was used.

## III. RESULTS AND DISCUSSION

### A. Characterization of Configurations

Since there are two sub-lattices within the ordered "anti-ferromagnetic" structure on the square lattice, there will also be two possible variants for the ordered phase, one where the A-atoms are on the even sub-lattice (which we call for short the even variant) and one where the A-atoms are on the odd sub-lattice (odd variant). To represent "snap-shot" pictures of the configurations in a way that clearly differentiates between the two variant ordered phases as well as the disordered phase, we put a solid square at an even site occupied by an A-particle and an open circle at an odd site occupied by an A-particle. The sites occupied by the B-particles are left empty see Fig. 2.

We define the short range order parameter $\eta_{\mathrm{sr}}$,

$$\eta_{\mathrm{sr}} = \frac{1}{2} - \frac{1}{4N} \sum_{\mathbf{p} \in \mathscr{L}} \sum_{j=1,2} \gamma(\mathbf{p})\, \gamma(\mathbf{p} + a\mathbf{e}_j) \tag{6}$$

and the long range order parameter $\eta_{\mathrm{lr}}$,

$$\eta_{\mathrm{lr}} = \frac{1}{N} \sum_{\mathbf{p} \in \mathscr{L}} \gamma(\mathbf{p})(-1)^{p_1 + p_2} \tag{7}$$

$\eta_{\mathrm{sr}}$ represents the relative amount of the ordered phase, irrespective of whether the order corresponds to the odd or the even variant, while $\eta_{\mathrm{lr}}$ is the global average of the staggered spin variable and corresponds to twice the difference in the concentration of A-atoms on the odd and the even sub-lattice.

Our first observation is that the short-range ordering of the domains takes place quite rapidly. We find that $|\eta_{\mathrm{sr}}/2c - 1| < 10^{-2}$ after $10^3$ MCS. To characterize the decomposition kinetics, we use the structure function

$$S_{\mathbf{k}} = \frac{1}{N} \left| \sum_{\mathbf{p} \in \mathscr{L}} \exp(i\mathbf{k} \cdot \mathbf{p})\, \gamma(\mathbf{p}) \right|^2 \tag{8}$$

where $\mathbf{k} = (k_1, k_2)$ is a reciprocal lattice vector, with $k_j = 2\pi K_j / La$ and $K_j = 1, 2, \ldots, L$ for $j = 1, 2$. For a system undergoing both ordering and decomposition, the structure function is concentrated in two areas, around the point $(\pi/a, \pi/a)$ (related to ordering) and around the point $(0, 0)$ (related to decomposition) of reciprocal space. Note, that $S_{(0,0)} = N(1-2c)^2$ and that $S_{(\pi,\pi)} = N\eta_{\mathrm{lr}}^2$.

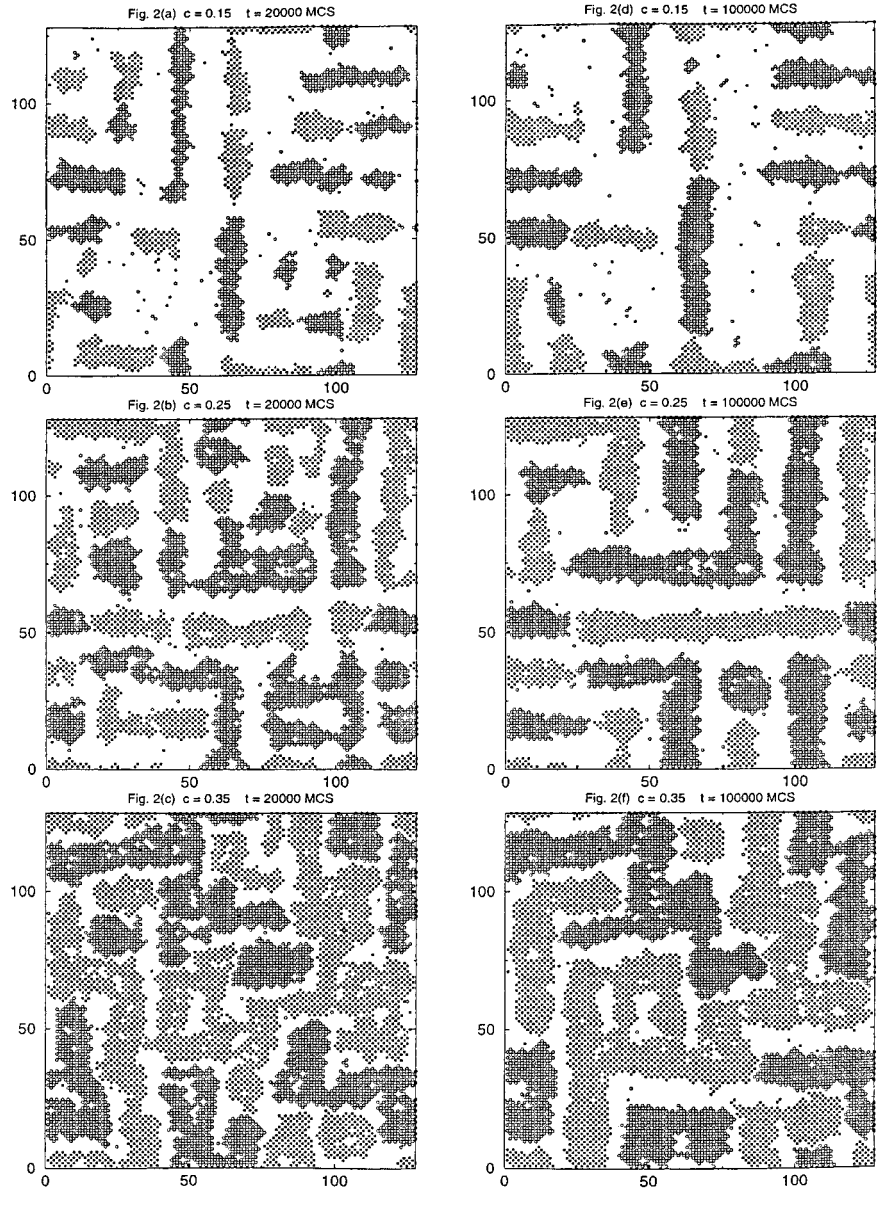


Fig. 2. Configurations after 20000 MCS for $c = 0.15$ (a), $c = 0.25$ (b) and $c = 0.35$ (c) and after 100000 MCS for $c = 0.15$ (d), $c = 0.25$ (e) and $c = 0.35$ (f). $c = 0.25$ is the (approximate) tricritical concentration. The symbols show the occupancy of the even sites (full symbols) and of the odd sites (open symbols) by the particles with positive spins. There was no external stress applied ($\zeta = 0$).

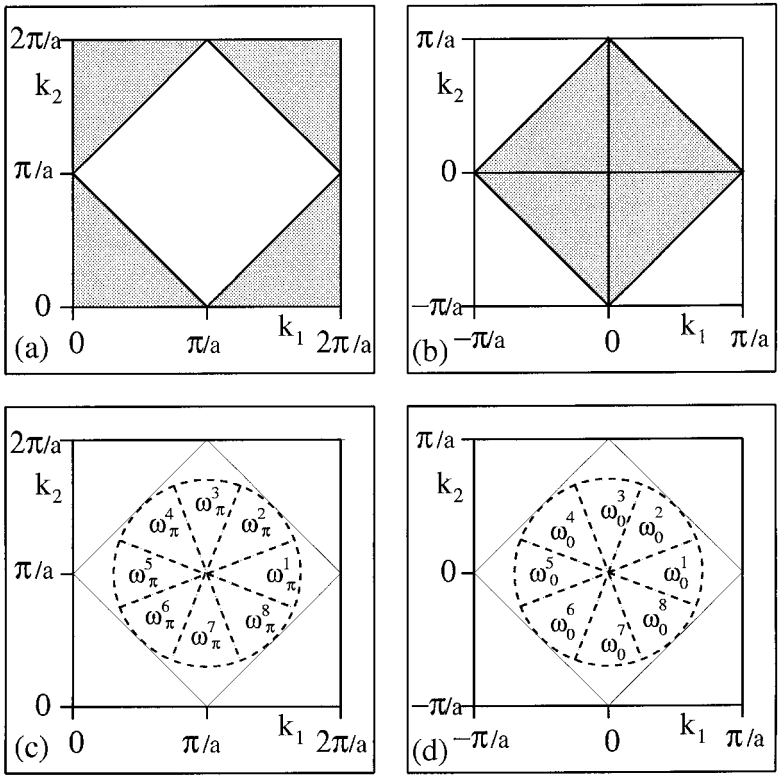


Fig. 3. Decomposition of the first Brillouin zone into $\Omega_0$ (grey area) and $\Omega_\pi$ (white area) centered around $\mathbf{k} = (\pi/a, \pi/a)$ (a) and around $\mathbf{k} = (0, 0)$ (b). The dashed lines in (c) and (d) sketch the **k**-space decomposition around $\mathbf{k} = (\pi/a, \pi/a)$ (c) and around $\mathbf{k} = (0, 0)$ (d) according to Eq. (16).

To study the kinetics and scaling properties of the two processes we divide as in ref. 11 the (square shaped) Brillouin zone in reciprocal space into two regions of equal area (see Fig. 3): a diamond centered at $(0, 0)$ describing decomposition,

$$\Omega_0 = \{\mathbf{k}\colon |k_1| + |k_2| \leqslant \pi/a\} \tag{9}$$

and a region consisting of four triangles. Under the periodicity of the reciprocal lattice the points of the latter region are together equivalent to a second diamond-shaped region $\Omega_\pi$ in reciprocal space centered around $(\pi/a, \pi/a)$,

$$\Omega_\pi = \{\mathbf{k}\colon |k_1 - \pi/a| + |k_2 - \pi/a| \leqslant \pi/a\} \tag{10}$$

describing ordering. To test scaling behavior of the structure function, we average it over directions within the two squares $\Omega_\nu$ related to ordering ($\nu = \pi$) and to decomposition ($\nu = 0$), separately. We define:

$$S_\nu(k) = \sum_{\Delta_\nu(k)} S_{\mathbf{k}'} \Big/ \sum_{\Delta_\nu(k)} 1 \tag{11}$$

where

$$\Delta_\nu(k) = \{\mathbf{k}' : k - \delta k < |\mathbf{k}' - (\nu, \nu)/a| \leqslant k + \delta k\} \tag{12}$$

is a ring of width $2\delta k$, $\delta k = \pi/La$, and median radius $k = |\mathbf{k}| = (k_1^2 + k_2^2)^{1/2} = 2\pi K/La$, $K = 1, 2, \ldots, [L/2\sqrt{2}]$. Since the configurations on the lattice are evolving with time, we are also using the notation $S_\nu(k, t)$ for the directionally averaged structure function computed from the configuration at time $t$.

The scaling hypothesis for the late stages of coarsening, in systems undergoing either phase segregation or ordering, is that the system is characterized by a single length scale $\lambda(t)$. This means in particular that for values of $k^{-1}$ which are large compared to the lattice spacing and small compared to the size of the system $S(k, t)$ should (up to a time dependent factor) be a function of only one variable, $\lambda(t)\, k$. In our case we need a priori two characteristic lengths, $\lambda_\nu(t)$, $\nu = 0, \pi$. We therefore hypothesize that for the system under consideration

$$\tilde{S}_\nu(k, t) \approx d_\nu(t)\, F_\nu(k\lambda_\nu(t)) \qquad \text{as} \quad t \to \infty \tag{13}$$

where $\tilde{S}_\nu(k, t)$ is, for fixed $k \neq 0$, the macroscopic (formally the infinite volume) limit of the corresponding directionally averaged structure function at time $t$:

$$S_\nu(k, t) \to \tilde{S}_\nu(k, t) \qquad \text{as} \quad L \to \infty \tag{14}$$

To test the generalized scaling hypothesis (13) we defined, following common practice for systems in which there is only one scaling length,

$$\lambda_\nu^{-1}(t)\, 2\pi \equiv k_\nu(t) = \sum_k k S_\nu(k, t) \Big/ \sum_k S_\nu(k, t), \qquad k = 2\pi K/La \tag{15}$$

The results are shown in Fig. 4(a) and (b). For times greater than $2 \times 10^4$ the growth of these length scales is well described by a time evolution of the type: $\lambda_\nu = a_\nu + b_\nu t^{1/3}$, see below. Due to the EI the ordered domains are oriented preferentially parallel to the coordinate axis. In order to quantify

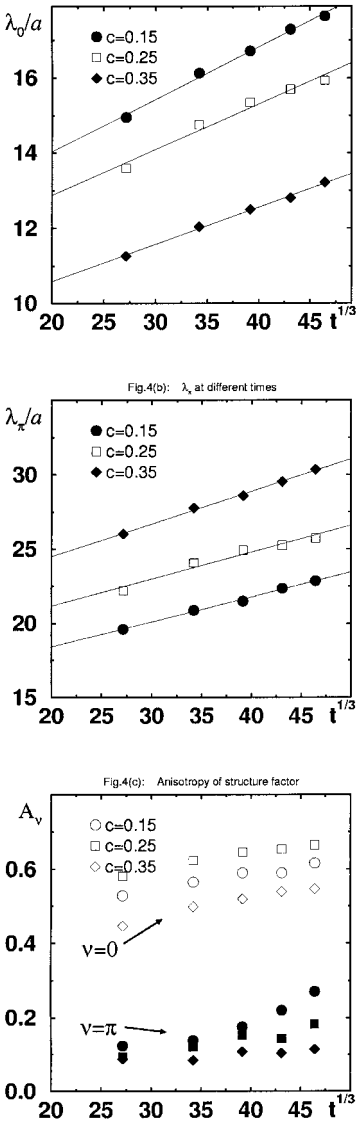


Fig. 4. Inverse first moments of the structure factors around $(0, 0)$ and $(\pi/a, \pi/a)$, $\lambda_0$ (a) and $\lambda_\pi$ (b) versus $t^{1/3}$. The slopes of the fitting lines in (a) are: $b_0/a = 0.14$, 0.12, 0.1 (from top to bottom), the slopes of the lines in (b) are: $b_\pi/a = 0.22$, 0.18, 0.17 (from top to bottom). (c) shows the anisotropy factors $A_0$ and $A_\pi$ versus $t^{1/3}$ (in units of MCS) for different concentrations. $A_v = 0$ corresponds to an isotropic situation and $A_v = 1$ corresponds to a situation where the structure factor is concentrated on the $k_x = 0$ and the $k_y = 0$-lines.

the amount of anisotropy in the resulting structure factor we divide the **k**-space around (0, 0) and $(\pi/a, \pi/a)$ into eight regions $\omega_v^I$, $(I = 1, 2, ..., 8)$, which are centered around the diagonals and the axes (see Fig. 3):

$$\omega_v^I := \left\{ \mathbf{k}: |a\mathbf{k} - (v, v)| < \frac{\pi}{\sqrt{2}},\ -\frac{3\pi}{8} + I\frac{\pi}{4} \leqslant \arctan\frac{ak_2 - v}{ak_1 - v} \leqslant -\frac{\pi}{8} + I\frac{\pi}{4} \right\},$$
$$I = 1, 2, ..., 8 \tag{16}$$

The contributions of the structure factor in the regions around the axes (odd $I$) is weighted by a "+" sign, and from the regions around the diagonals with a "−." The sum of these terms gives the anisotropy factor $A_v$:

$$A_v = \sum_{I=1}^{8} (-1)^I \left[ \sum_{\omega_v^I} S_{\mathbf{k}} \Big/ \sum_{\omega_v^I} 1 \right] \tag{17}$$

For spherically symmetric structure factors, $A_v = 0$; in the case of ordering with structures parallel to the coordinate axes, $A_v > 0$.

## B. Domain Morphology

We consider now the domain morphology and the growth kinetics of the system for choices of the temperature and concentration, which place the system well below the tricritical temperature in the coexistence region.

As already noted, the first stage of the kinetics is given by a fast ordering in small domains on the even and odd sub-lattices. Typical configurations after 20000 MCS are shown in Fig. 2 (a)–(c) for $c = 0.15$, $c = 0.25$ and $c = 0.35$. Configurations after 100000 MCS are shown in Fig. 2 (d)–(f) for the same parameters as in Fig. 2 (a)–(c). Due to the coarsening process the ordered domains have grown. For the two small concentrations the growth in the long direction has partly stopped where domains which are ordered on different sub-lattices collide. An APB blocks further growth of the domains. For $c = 0.35$, 70% of the lattice sites are parts of ordered domains. Here many APB's appear already at an early stage of the decomposition which slow down the dynamics. The presence of these narrow channels subdividing the plates (or stripes) in sub-domains is a difference to the situation of the FM case with EI's.[37, 38] Such channels are typically observed in nickel base superalloys where the precipitates are ordered.[21] In the present model neighboring sub-domains are ordered on a different sub-lattice which means that the narrow channels are, in fact, wetted APB's. This is in good agreement with Khachaturyan's assumption.[31]

In Fig. 4 we show the corresponding length scales $\lambda_0$ for the decomposition and $\lambda_\pi$ for the ordering as a function of the time. $\lambda_\pi$ is always larger than $\lambda_0$, $\lambda_0$ decreases with the concentration, whereas $\lambda_\pi$ increases with $c$. To explain this behavior we note that for the higher concentration the ordered domains contain more particles than for smaller concentrations and thus $\lambda_\pi$, which is a measure for the average size of the ordered domains, is increasing with the concentration. On the other hand, due to the increase in APB area the decomposition process is hindered with increasing concentration. Thus $\lambda_0$, which is a measure for a typical "wave length" of the separated regions in the system, is decreasing with $c$. This is again in contrast to the FM case,[37, 38] where a concentration $c$ and $1-c$ of a given phase are equivalent. However, a monotonic dependence on the amount of ordered phase had also been found in the AFM case without EI's.[11] It is, therefore, very likely that the slowing down of the kinetics with increasing amount of ordered phase is related to the presence of APB's which are not very mobile. All length scales, however, can be well described by a linear dependence on $t^{1/3}$, which may be due to the increasing width of the structures which is not affected by APB's as much as the growth in length. The wide channels between neighbouring stripes were already found in the FM case with EI's[37, 38] and are probably due to an effective repulsion of the stripes due to the EI. This also means that neighbouring ordered stripes are not necessarily on different sub-lattices. The growth in thickness is, therefore, unrelated to APB's and similar in the FM and AFM case.

The anisotropy of the structure factor is shown in Fig. 4c. For $v=0$ (open symbols), it reflects the stripe-like character of the domains induced by EI. In agreement with previous simulation work on the coarsening of (non-ordered) domains under the influence of EI,[36] the anisotropy is largest for an equal amount of the two phases. This shows that—while being crucial for the kinetics of coarsening—the atomic ordering in one of the phases has only a small influence on the development of domain shape anisotropy. This is emphasized by the fact that the ordering parameter (as measured by the structure function close to $v=\pi$) shows only little anisotropy (Fig. 4c, full symbols).

In order to analyze the difference between the structure of the ordered and the disordered regions for lattice fractions which are symmetric about $c=0.25$, we show in Fig. 5(a) configurations after 100000 MCS for $c=0.35$, where 70% of the particles are in ordered regions. In this figure the ordered regions are plotted white and the disordered black. For comparison with this situation we show configurations for $c=0.15$ in Fig. 5(b) and (c), where 30% of the particles are in ordered regions. In order to make visible the differences of the domain structure in the three cases, the

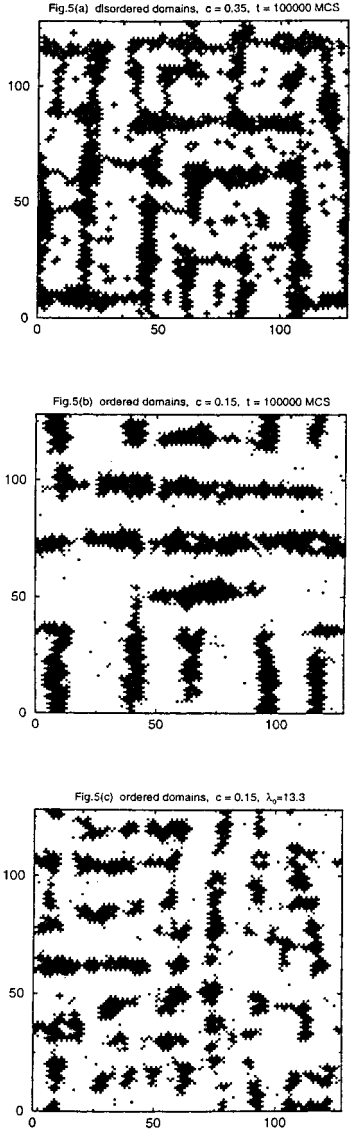


Fig. 5. (a) corresponds to the situation of 70% ordered phase and 30% disordered phase, full symbols show the *disordered* domains for $c = 0.35$ after 100000 MCS after which $\lambda_0 = 13.4a$, (b) corresponds to the situation of 30% ordered phase and 70% disordered phase after the time as in (a), the full symbols show the *ordered* domains for $c = 0.15$ after 100000 MCS, (c) corresponds to the same situation as in (b) but after a time (10000 MCS), where the domains size is the same as in (a) ($\lambda_0 = 13.3a$).

ordered regions in (b) and (c) are shown in black and the disordered regions white. In Fig. 5(b) the same number of MCS has been considered as in (a), and in (c) a configuration has been selected, for which the characteristic length scale $\lambda_0$ agrees with the value in (a). In both figures, (b) and (c), the morphologies of the ordered domains differ significantly from the morphology of the disordered domains in (a). Such an effect has been previously found in a model with AFM ordering[11] but no EI and was assumed to be due to APB's between ordered domains on different sub-lattices, wetted by the disordered phase. In the present case, a similar wetting of APB's was observed.

## C. Growth Kinetics and Scaling

The two characteristic length scales related to ordering and decompositions, $\lambda_v(t)$, have been computed using Eq. (15). Figures 4(a) and (b) show that for times greater than $2 \times 10^4$ the growth of these length scales is well described by a time evolution of the type:

$$\lambda_v = a_v + b_v t^{1/3} \tag{18}$$

Despite the fact that the structure function showed considerable anisotropy, we considered a scaling hypothesis for the directionally averaged structure function (where the anisotropy has vanished due to averaging) in the form

$$S_v(k, t) \approx B_v k_v(t)^{-2} F_v(k/k_v(t)) \tag{19}$$

where $2\pi/k_v(t) = \lambda_v(t) = a_v + b_v t^{1/3}$. A standard way to choose the constants $a_0$ and $B_0$ is to require that the scaling function $F_0$ satisfy the normalization condition $\max[F_0(x)] = F_0(1) = 1$. This permits comparison of characteristic parameters at different concentrations.

In Fig. 6 we show the scaling plots of $F_0$ for the directionally averaged structure factor $S_0(k, t)$, where the free coefficients have been chosen such that the maximum of $F_0$ is at $x = 1$ and $F_0(1) \approx 1$. For all three concentrations we find a reasonably good scaling behavior, supporting the scaling hypothesis.

Several interesting features of the directionally averaged structure function are visible in Fig. 6. First, in Fig. 6a and—more prominently—in Fig. 6c a shoulder or secondary maximum is visible around $x = 2$. This can be interpreted as a second order of the main peak at $x = 1$[36] and results from a degree of ordering in the spatial distribution of the domains considerably higher than in phase separation without EI, where such a

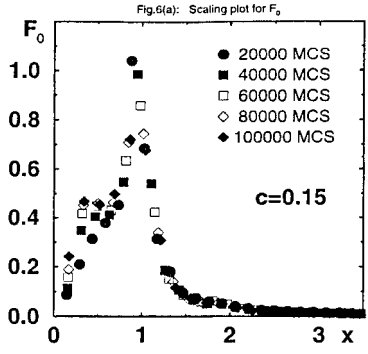


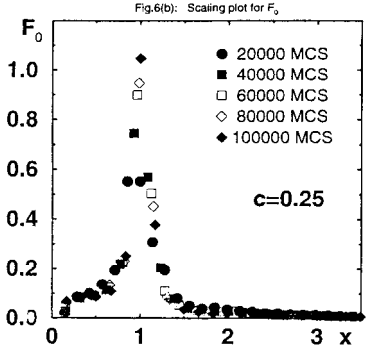


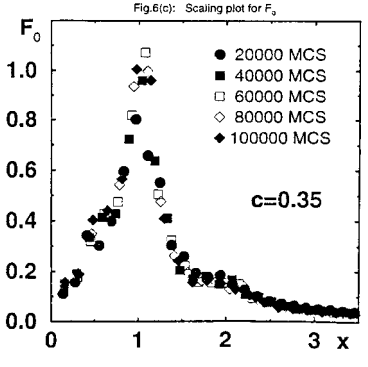


Fig. 6. Spherically averaged structure function for decomposition rescaled with $\lambda_0$, $F_0(k/k_0)$ for $c = 0.15$ (a), $c = 0.25$ (b) and $c = 0.35$ (c). Note the shoulders around $x = 2$ in (a) and (c).

secondary maximum does not usually occur.[10, 11] For the same reason, the main peak at $x = 1$ is narrower than in cases without EI. This last effect is even more pronounced for the symmetric alloy composition ($c = 0.25$, see Fig. 6b). Despite this, there is no secondary maximum in this case. As discussed earlier,[36] this occurs because in a succession of stripes with equal thickness, all even (and, in particular, the second) order peaks are suppressed. This does not occur in Fig. 6a and 6c, because the ordered and disordered domains have different thickness (due to the asymmetric composition, see Fig. 2).

## D. Rafting

Directional coarsening ("rafting") is a well-known phenomenon, observed when alloys containing misfitting precipitates are subjected to uniaxial external load. Morphologies with plate-like structures perpendicular or rod-like structures parallel to the stress directions may develop. This phenomenon has been studied by experimental methods as well as with MC simulations. In the latter[37, 38] a ferromagnetic interaction has been considered which does not lead to ordering on different sub-lattices and APB's discussed in the present work.

We studied the influence of uniaxial external tensile stress in the $x$-direction ($\zeta = 0.1$) on the morphologies. In Fig. 7 we present the resulting configurations 100000 MCS after a quench into the coexistence region for different concentrations of the A-particles. As in the case with FM interactions[37, 38] the ordered domains align parallel to the $x$-axis. The structures may consist of ordered domains extending over the full length of the simulation box or may consist of domains ordered on different sub-lattices intersected by APB's. Independent of these structural details, for small concentrations $c$ (see Fig. 7 (a) and (b)) these structures contain a "waviness" similar to the phenomenon found in the study with FM interaction. For larger $c$ (see Fig. 7(c)) the "waviness" is less pronounced since neighboring ordered regions in y-direction have smaller average distances compared to the case with smaller $c$-values, consequently either compact ordered domains are formed which are separated by horizontal disordered stripes, or APB's appear in $y$-direction, both effects hinder the appearance of wave-like structures.

## IV. CONCLUDING REMARKS

In this paper, we studied the coarsening of anti-ferromagnetically ordered domains under the influence of elastic misfit interactions with and without externally applied uniaxial stress.

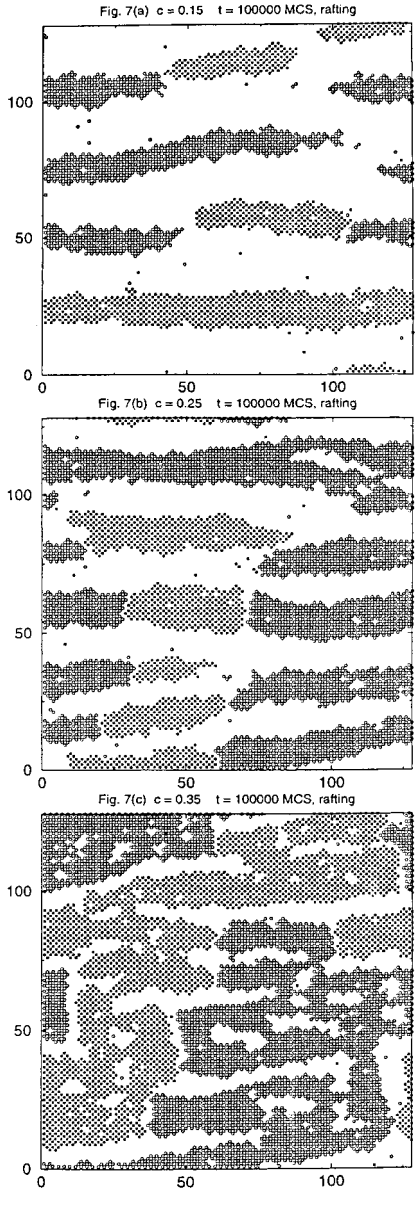


Fig. 7. Configurations due to rafting with uniaxial external tensile stress in $x$-direction ($\zeta = 0.1$) after 100000 MCS with a random solution as a starting configuration for $c = 0.15$ (a), $c = 0.25$ (b) and $c = 0.35$ (c). Full symbols show the occupancy of the even sites and open symbols the occupancy of the odd sites by the particles with positive spins.

• As expected, the EI led to the development of a platelet morphology consisting of two types of ordered domains (differing by a phase) and a disordered domain.

• Characteristic lengths associated to these domains follow a law of the type $R = a_v + b_v t^{1/3}$ with $v = 0, \pi$ referring to decomposition and ordering structure functions.

• We observed the presence of narrow channels subdividing the ordered plates (or stripes) into sub-domains. Such channels are typically observed in Nickel base superalloys where the precipitates are ordered. It was commonly found that neighboring subdomains are ordered on a different sub-lattice which means that the narrow channels are, in fact, wetted

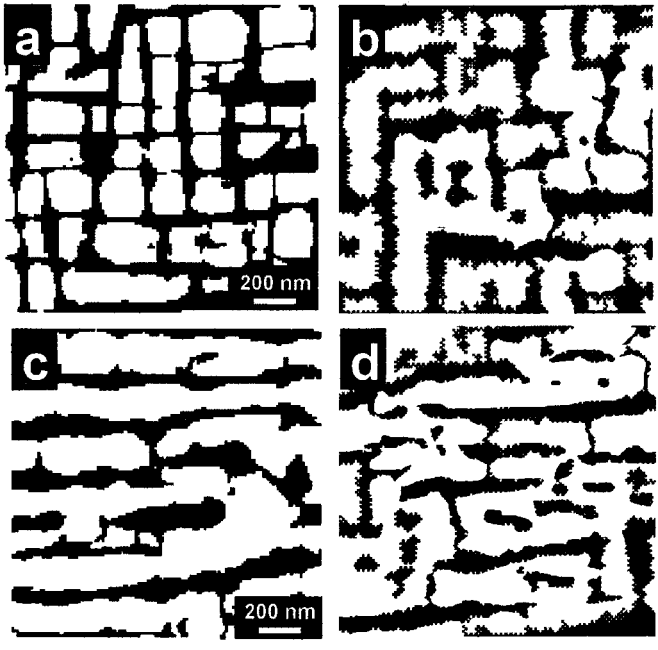


Fig. 8. (a) Transmission electron microscopic image of Ni-Al-Mo alloy with Mo-composition chosen such as to make the lattice spacing in the precipitates (gamma-prime phase) smaller than in the disordered matrix (misfit $-0.5\%$). Treatment: 5h at 1253 K (Orientation 001). One observes cube-like precipitates, aligned along the elastically soft directions, [010] and [100] (From ref. 21). (b) Data from Fig. 2f replotted with the convention that the disordered phase is shown black, while both variants of the ordered phase are shown in white. (c) Transmission electron microscopic image of the same Ni-Al-Mo alloy as in (a). Same thermal treatment as in (a) but now with a external compressive load of 130 MPa applied to it along the vertical [010]-direction. (From ref. 21). (d) Data from Fig. 7c replotted with the same convention as in (b).

APB's. This is in good agreement with Khachaturyan's ideas.[31] We believe that the APB's are responsible for the morphology with 30% ordered phase in the disordered matrix being quite different from that with 30% disordered phase (Such an effect was also found earlier in this AFM model with no EI but is absent in FM systems.) In fact the main difference in the kinetics and morphologies, between the present AFM model and the previously studied FM ones appears to be due to the presence of the APB.

• Since these APB's only disappear when two of them meet and annihilate, it is very difficult for neighbouring sub-domains to join up into a single domain. Hence, the growth kinetics is hindered by the presence of the APB's and this is responsible for the coefficient $b_0$ and thus the average domain size was found to decrease monotonically with the amount of ordered phase (varying from 30% to 70%).

• The wide channels between neighbouring stripes also found in the FM case are probably due to an effective repulsion of the stripes due to the EI. This means that neighbouring ordered stripes are not necessarily on different sub-lattices. The growth in thickness is, therefore, unrelated to APB's.

• The effect of uniaxial external stress is to cause "rafting" of the domains. The APB's cause the stripes to be segmented.

• Finally we mention the great similarity between the morphologies obtained from our simulations and those obtained from experiment (despite the great difference in scales) once the distinction between the differently ordered subdomains (not distinguished in the experiments) is removed from the simulation output; see Fig. 8. This compares our data with transmission electron micro-graphs of Ni-Al-Mo alloys annealed with and without external stress.

## ACKNOWLEDGMENTS

P.N. thanks the DFG for financial support (Heisenberg foundation and SFB 513). The computations were in part carried out on the CRAY T3E and CRAY T90 at the HLRZ. The work of J.L.L. was supported in part by NSF Grant NSF-DMR 95-23266. We thank V. Gorentsveig and (ref.) for useful comments.

## REFERENCES

1. J. W. Cahn, *Acta Metall.* **9**:795 (1961); **10**:179 (1962).
2. A. B. Bortz, M. H. Kalos, J. L. Lebowitz, and M. H. Zendejas, *Phys. Rev. B* **10**:535 (1974); J. Marro, A. B. Bortz, M. H. Kalos and J. L. Lebowitz, *Phys. Rev. B* **12**:2000 (1975).

3. J. D. Gunton, M. San Miguel, and P. S. Sahni, in *Phase Transitions and Critical Phenomena*, C. Domb and J. L. Lebowitz, eds. (Academic Press, New York, 1983), Vol. 8.
4. K. Binder, in *Materials Science and Technology*, P. Haasen, ed. (VCH, Weinheim, 1991), Vol. 5, Chap. 7.
5. R. Wagner and R. Kampmann, in *Phase Transformations in Materials*, P. Haasen, ed. (VCH, Weinheim, 1991), Vol. 5, Chap. 4.
6. A. G. Khachaturyan, *Theory of Structural Transformations in Solids* (Wiley, New York, 1983).
7. J. Marro, J. L. Lebowitz, and M. H. Kalos, *Phys. Rev. Lett.* **43**: 282 (1979); J. L. Lebowitz, J. Marro, and M. H. Kalos, *Acta Metall.* **30**:297 (1982); P. Fratzl, J. L. Lebowitz, J. Marro, and M. H. Kalos, *Acta Metall.* **31**:1849 (1983).
8. I. M. Lifshitz and V. V. Slyozov, *J. Phys. Chem. Solids* **19**:35 (1961); C. Wagner, *Z. Elektrochem.* **65**:581 (1961).
9. P. Fratzl, J. L. Lebowitz, O. Penrose, and J. Amar, *Phys. Rev. B* **44**:4794 (1991).
10. P. Fratzl and J. L. Lebowitz, *Acta Metall.* **37**:3245 (1989).
11. V. I. Gorentsveig, P. Fratzl, and J. L. Lebowitz, *Phys. Rev.* **55**:2912 (1997).
12. J. K. Tien and S. M. Copley, *Metall. Trans.* **2**:215 (1971).
13. For a recent short review see, e.g., S. Socrate and D. M. Parks, *Acta Metall. Mater.* **41**:2185 (1993).
14. Linear elastic models for rafting are reviewed in: J. C. Chang and S. M. Allen, *J. Mater. Res.* **6**:1843 (1991).
15. T. Miyazaki, K. Nakamura, and H. Mori, *J. Mater. Sci.* **14**:1827 (1979).
16. M. V. Nathal, R. A. MacKay, and R. V. Miner, *Metall. Trans. A* **20**:133 (1989).
17. M. Feller-Kniepmeier and T. Link, *Metall. Trans. A* **20**:1233 (1989).
18. C. Carry and J. L. Strudel, *Acta Metall.* **25**:767 (1977); **26**:859 (1978).
19. T. M. Pollock and A. S. Argon, *Acta Metall. Mater.* **42**:1859 (1994).
20. J. Y. Buffiere and M. Ignat, *Acta Metall. Mater.* **43**:1791 (1995).
21. O. Paris, M. Fährmann, E. Fährmann, T. M. Pollock, and P. Fratzl, *Acta Mater.* **45**:1085 (1997).
22. T. Miyazaki, M. Doi, and T. Kozaki, *Solid State Phen.* **3**:158 (1988); T. Miyazaki and M. Doi, *Mater. Sci. Eng. A* **110**:175 (1989).
23. A. Maheshwari and A. J. Ardell, *Phys. Rev. Lett.* **70**:2305 (1993).
24. O. Paris, M. Fährmann, and P. Fratzl, *Phys. Rev. Lett.* **75**:3458 (1995).
25. A. D. Sequeira, H. A. Calderon, G. Kostorz, and J. A. Pedersen, *Acta Metall. Mater.* **43**:3427 (1995); **43**:3441 (1995).
26. M. Fährmann, P. Fratzl, O. Paris, E. Fährmann, and W. C. Johnson, *Acta Metall. Mater.*, **43**:1007 (1995).
27. P. Fratzl, F. Langmayr, G. Vogl, and W. Miekeley, *Acta Metall. Mater.* **39**:753 (1991); F. Langmayr, P. Fratzl, G. Vogl, and W. Miekeley, *Phys. Rev. B* **49**:11759 (1994).
28. J. D. Eshelby, *Prog. Solid Mech.* **2**:89 (1961); Ardell, R. B. Nicholson, and J.D. Eshelby, *Acta metall.* **14**:1295 (1966).
29. A. Onuki and H. Nishimori, *Phys. Rev. B* **43**:13649 (1991); H. Nishimori and A. Onuki, *Phys. Rev. B* **42**:980 (1990).
30. Y. Wang, L. Q. Chen, and A. G. Khachaturyan, *Acta Metall. Mater.* **41**:279 (1993); Y. Wang and A. G. Khachaturyan, *Acta Metall. Mater.* **43**:1837 (1995).
31. Y. Wang and A. G. Khachaturyan, *Scripta Metall. Mater.* **31**:1425 (1994).
32. W. C. Johnson, *Acta metall.* **32**:465 (1984); T. A. Abinandanan and W. C. Johnson, *Acta Metall. Mater.* **41**:17 (1993).
33. P. W. Voorhees, G. B. McFadden, and W. C. Johnson, *Acta Metall. Mater.* **40**:2979 (1992).

34. K. Kawasaki and Y. Enomoto, *Physica A* **150**:463 (1988); Y. Enomoto and K. Kawasaki, *Acta Metall.* **37**:1399 (1989).
35. P. Fratzl and O. Penrose, *Acta Metall. Mater.* **43**:2921 (1995).
36. P. Fratzl and O. Penrose, *Acta Mater.* **44**:3227 (1996).
37. C. L. Laberge, P. Fratzl, and J. L. Lebowitz, *Phys. Rev. Lett.* **75**:4448 (1995).
38. C. L. Laberge, P. Fratzl, and J. L. Lebowitz, *Acta Mater.* **45**:3949 (1997).
39. W. A. Soffa and D. E. Laughlin, *Acta Metall.* **37**:3019 (1989).
40. A. Pineau, *Acta Metall.* **24**:559 (1976).
41. W. C. Johnson, M. B. Birkenpas, and D. E. Laughlin, *Acta Metall.* **36**:3149 (1988).
42. C. Sagui, A. M. Somoza, and R. C. Desai, *Phys. Rev. E* **50**:4865 (1994).
43. J. Gayda and D. J. Srolovitz, *Acta Metall.* **37**:641 (1989).
44. D. P. Landau, *J. Appl. Phys.* **42**:1284 (1971).
45. D. P. Landau, *Phys. Rev. Lett.* **28**:449 (1972).
46. J. M. Kincaid and E. G. D. Cohen, *Phys. Reports* **22**:57 (1975).
47. A. G. Khachaturyan, *Soviet Phys. Crystallogr.* **10**:256 (1965).
48. H. E. Cook and D. DeFontaine, *Acta Metall.* **17**:915 (1969).